Appl Magn Reson (2017) 48:175–200
DOI 10.1007/s00723-016-0854-9

Applied Magnetic Resonance

ORIGINAL PAPER

EPR Line Shifts and Line Shape Changes Due to Spin Exchange Between Nitroxide Free Radicals in Liquids 10. Spin-Exchange Frequencies of the Order of the Nitrogen Hyperfine Interaction: A Hypothesis

Barney L. Bales[1] · **Miroslav Peric**[1]

Received: 19 October 2016 / Revised: 19 November 2016 / Published online: 3 December 2016

Abstract The behavior of electron paramagnetic resonance spectra due to ^{15}N and ^{14}N nitroxide free radicals undergoing spin exchange in liquids at frequencies ω_{ex} that are high, of the same order of magnitude as the nitrogen hyperfine coupling constant A_0, is investigated. The well-known features are reconfirmed: (1) at low values of ω_{ex} where the lines broaden, shift toward the center of the spectrum, and change shape due to the introduction of a resonance of the form of a dispersion component; (2) at values of ω_{ex} comparable to A_0, where the lines merge into one; and (3) at values much larger than A_0, where the merged line narrows. It is found that each line of a spectrum may be decomposed into an admixture of a single absorption and a single dispersion component of Lorentzian shape. These two- or three-line absorption–dispersion admixtures, for ^{15}N and ^{14}N, respectively, retain their individual identities even after the spectrum has merged and has begun to narrow. For both isotopes, the average broadening and integrated intensities are equal to the predictions of perturbation theory although, in the case of ^{14}N, the outer lines broaden faster than the central line and intensity moves from the outer lines to the central line. In fact, the outer line intensity becomes zero and then negative at higher values of ω_{ex} which is compensated by the central line becoming more intense than the overall integrated intensity. For both isotopes, the dispersion components and the line shifts depart from the perturbation predictions. The results are presented in terms of measurable quantities normalized to A_0 so that they may be applied to any two- or three-line spectrum.

✉ Barney L. Bales
barney.bales@csun.edu

Miroslav Peric
miroslav.peric@csun.edu

[1] Department of Physics and Astronomy, The Center for Biological Physics, California State University at Northridge, Northridge, CA 91330, USA

1 Introduction

This is a continuation of a series of articles started with the ultimate goal to measure translational diffusion of nitroxide free radicals (nitroxides) in supramolecular structures in solution exploiting electron paramagnetic resonance (EPR) spectral changes under the influence of Heisenberg spin exchange (HSE) [1]. EPR spectra of nitroxides in low-viscosity liquids may be simple two-, three-, or five-line spectra in the absence of further hyperfine structure. Call this Case 1. For Case 2, in which hyperfine structure due to protons or deuterons is significant, the spectra may be complicated, with hundreds of lines [2]. In the absence of HSE, denote the line spacing due to nitrogen hyperfine coupling by A_0 and average spacing due to the protons or deuterons, by $<a_0>$. We restrict our discussion to cases in which the HSE is strong which means that during the brief time that two nitroxides are in intimate contact, τ_c, under the influence of an average exchange integral, $|J|$, that the product is much larger than unity; i.e., $|J|\tau_c \gg 1$. Strong exchange has been found to be fulfilled for nitroxides in most cases [3]

For Case 1, spectral changes due to HSE at increasing spin-exchange frequency, ω_{ex}, are as follows: for $\omega_{ex}/\gamma \ll A_0$, where γ is the gyromagnetic ratio of the electron, the lines (a) broaden, (b) shift toward the center of the spectrum, and (c) change shape due to the introduction of HSE-induced dispersion. For $\omega_{ex}/\gamma \approx A_0$, the lines (d) collapse to a single line; and for $\omega_{ex}/\gamma \ll A_0$, (e) the single line narrows [3].

For Case 2, for $\omega_{ex}/\gamma \ll <a_0>$, the lines shift to the center of each proton (deuteron) hyperfine multiplet as the multiplets shift to the center of the spectrum, for $\omega_{ex}/\gamma \approx <a_0>$, the multiplets merge into inhomogeneously broadened lines; and for $\omega_{ex}/\gamma \ll <a_0>$, the multiplets narrow at which point, Case 2 is identical to Case 1. For nitroxides, $<a_0>$ is typically 0.1–0.4 G, while A_0 is 14–24 G [1]; thus, it is easy to find experimental conditions that fulfill both $\omega_{ex}/\gamma \gg <a_0>$ and $\omega_{ex}/\gamma \ll A_0$. For ω_{ex} larger than this, all nitroxides may be treated as Case 1; thus, we restrict this presentation to Case 1.

The spin-exchange frequency is often written in terms of the spin-exchange rate constant, K_{ex}, as $\omega_{ex} = c \cdot K_{ex}$ [3], where c is the concentration in mol/L. Thus, ω_{ex} may be varied experimentally by varying the nitroxide concentration. Thus, a limit of $\omega_{ex} \to 0$ may be achieved by taking the limit $c \to 0$. Therefore, when we speak of the absence of HSE, we mean either $\omega_{ex} \to 0$ or $c \to 0$. We consider only the case in which the microwave power is small enough to avoid saturation. The entire development is for first-derivative EPR spectra.

The generally accepted expression for the EPR spectrum is given by the derivative of the real part of Eq. (1) [3, 4]

$$Y(H) = \frac{I_{total}}{\pi} \frac{G(H)}{[1 - (\omega_{ex}/\gamma)G(H)]}, \tag{1}$$

where H is the magnetic field, I_{total} the integrated intensity, proportional to the number of spins, and $G(H)$ is given by:

$$G(H) = \sum_j \frac{\rho_j}{i(H - H_j) + \gamma^{-1}(\omega_{\text{ex}} + T_{2j}^{-1})}, \tag{2}$$

where the sum is over j which denotes the jth Lorentzian resonance line of degeneracy ρ_j at resonance field H_j with spin–spin relaxation time T_{2j}. Equation (1) is quite general [3], applicable to any number of lines; in this work, the sum is only over two (^{15}N) or three (^{14}N) lines. The peak-to-peak line width of line j in the absence of HSE is $\Delta H_{\text{ppj}}(0) = 2/\left(\gamma\sqrt{3}T_{2j}\right)$. For those readers who are familiar with a more phenomenological approach in which coupled equations are written in terms of relaxation times, see, for example, section 2.4 of Ref. [3] where an equation equivalent to Eq. (1) is derived.

Equation (1) does not include HSE that occurs during re-encounter collisions while two nitroxides reside within a cage [5].

For convenience, label the low-field line $j = +1$ and high-field $j = -1$ for both isotopes and the center line for ^{14}N $j = 0$.

The main purpose of this work is to carefully investigate intermediate spin exchange, $\omega_{\text{ex}}/\gamma \approx A_0$, for Case 1 and to hypothesize that Eq. (1) is equivalent to a sum over lines that are superpositions of absorption and dispersion Lorentzian line shapes.

Many of the conclusions that we reach here have been reported previously for two- [6], three- [7, 8], and five-line [9] spectra, but with considerably smaller values of $\omega_{\text{ex}}/\gamma A_0$. We find some rather unusual behavior of the line shapes as ω_{ex} increases through the intermediate spin-exchange region into the spin-exchange narrowing region.

2 Theory

2.1 Perturbation Theory in the Slow-Exchange Limit

The monograph [3] treated Eq. (1) with perturbation theory which predicted that at $\omega_{\text{ex}}/\gamma \ll A_0$, slow exchange, each line consisted of a superposition of an absorption and a dispersion function as follows [7]:

$$Y_j^{\text{pert}} = V_{\text{ppj}}^{\text{pert}}(\omega_{ex}) \cdot Abs_j^{\text{pert}} + V_{\text{dispj}}^{\text{pert}}(\omega_{\text{ex}}) \cdot \text{Disp}_j^{\text{pert}}, \tag{3}$$

where the superscript pert denotes the result from perturbation theory. The first-derivative Lorentzian absorption function of unit peak-to-peak intensity is given by [7]:

$$\text{Abs}_j^{\text{pert}} = \frac{-8\xi_j}{\left(3 + \xi_j^2\right)^2}, \tag{4}$$

and the first-derivative Lorentzian dispersion function of unit maximum intensity, by [7]:

$$\mathrm{Disp}_j^{\mathrm{pert}} = \frac{3\left(3-\xi_j^2\right)}{\left(3+\xi_j^2\right)^2}, \tag{5}$$

with

$$\xi_j = 2[H - H_j^{\mathrm{pert}}(\omega_{\mathrm{ex}})]/\Delta H_{\mathrm{pp}j}^{\mathrm{pert}}(\omega_{\mathrm{ex}}), \tag{6}$$

where $\Delta H_{\mathrm{pp}j}^{\mathrm{pert}}(\omega_{\mathrm{ex}})$ is the peak-to-peak line width [7]. The dependence of the functions and parameters in Eq. (3) on H and ω_{ex} is suppressed, except when they are needed for clarity. Thus, the slow-exchange spectrum consists of the sum [7]:

$$Y^{\mathrm{pert}} = \sum_j \left(V_{\mathrm{pp}j}^{\mathrm{pert}} \cdot \mathrm{Abs}_j^{\mathrm{pert}} + V_{\mathrm{disp}j}^{\mathrm{pert}} \cdot \mathrm{Disp}_j^{\mathrm{pert}}\right), \tag{7}$$

Line broadening due to HSE is defined by:

$$B_j \equiv \Delta H_{\mathrm{pp}j}(\omega_{\mathrm{ex}}) - \Delta H_{\mathrm{pp}j}(0), \tag{8}$$

Perturbation theory shows that the broadening is independent of j given by the following [7]:

$$B_j^{\mathrm{pert}} = \frac{2}{3}\frac{2}{\sqrt{3}}\omega_{\mathrm{ex}}/\gamma \quad \text{for } ^{14}\mathrm{N}, \tag{9a}$$

or

$$B_j^{\mathrm{pert}} = \frac{1}{2}\frac{2}{\sqrt{3}}\omega_{\mathrm{ex}}/\gamma \quad \text{for } ^{15}\mathrm{N}, \tag{9b}$$

The numerical factors 2/3 or 1/2 are the values of $1-\rho_j$, the fraction of spins with $j' \neq j$ [3].

For a Lorentzian line, the integrated intensity is given by [7]:

$$I_j = \frac{\pi}{\sqrt{3}}\left[\Delta H_{\mathrm{pp}j}\right]^2 V_{\mathrm{pp}j}, \tag{10}$$

In the slow-exchange limit, I_j is independent of j; all three (two) lines have the same integrated intensity; $I_j^{\mathrm{pert}} = I_{\mathrm{total}}/3$ or $I_j^{\mathrm{pert}} = I_{\mathrm{total}}/2$, respectively. Therefore [7],

$$V_{\mathrm{pp}j}^{\mathrm{pert}} = \frac{\sqrt{3}I_{\mathrm{total}}/3}{\pi\left[\frac{4\omega_{\mathrm{ex}}}{3\sqrt{3}\gamma} + \Delta H_{\mathrm{pp}}(0)_j\right]^2} \quad \text{For } ^{14}\mathrm{N}, \tag{11a}$$

$$V_{\mathrm{pp}j}^{\mathrm{pert}} = \frac{\sqrt{3}I_{\mathrm{total}}/2}{\pi\left[\frac{\omega_{\mathrm{ex}}}{\sqrt{3}\gamma} + \Delta H_{\mathrm{pp}}(0)_j\right]^2} \quad \text{For } ^{15}\mathrm{N}, \tag{11b}$$

For both isotopes [7],

$$V_{\mathrm{disp}j}^{\mathrm{pert}} = j\frac{4}{3\sqrt{3}}\frac{\omega_{ex}}{\gamma A_0}V_{\mathrm{pp}j}^{\mathrm{pert}}, \tag{12}$$

HSE leads to resonance field shifts of the outer lines toward the center as follows:

$$\delta H_j \equiv j[H(\omega_{ex})_j - H(0)_j] \geq 0, \tag{13}$$

These shifts are conveniently measured in terms of the differences in resonance fields of adjacent absorption lines, $A_{abs}(\omega_{ex})$ [6]:

$$A_{abs}(\omega_{ex}) = A_0 - \frac{1}{2}(\delta H_{+1} - \delta H_{-1}) \quad \text{for } ^{14}\text{N}, \tag{14a}$$

$$A_{abs}(\omega_{ex}) = A_0 - (\delta H_{+1} - \delta H_{-1}) \quad \text{for } ^{15}\text{N}, \tag{14b}$$

For slow exchange [6],

$$\frac{A_{abs}^{pert}(\omega_{ex})}{A_0} = 1 - \frac{1}{6}(\omega_{ex}/A_0\gamma)^2 \text{ for } ^{14}\text{N}, \tag{15a}$$

$$\frac{A_{abs}^{pert}(\omega_{ex})}{A_0} = 1 - \frac{1}{2}(\omega_{ex}/A_0\gamma)^2 \text{ for } ^{15}\text{N}, \tag{15b}$$

To simplify the presentation, we treat the case that the three (two) lines are of equal width in the absence of HSE; i.e., $\Delta H_{ppj}(0)$ is independent of j; in this case, V_{ppj} and $\Delta H_{ppj}(\omega_{ex})$ are symmetric about the spectrum center and the line shifts and the dispersion maxima are anti-symmetric: $\delta H_{+1} = -\delta H_{-1} \geq 0$ and $V_{disp+1}(\omega_{ex}) = -V_{disp-1}(\omega_{ex}) \geq 0$. For simplicity, we refer to either $V_{ppj}^{pert}(\omega_{ex})$ or $V_{dispj}^{pert}(\omega_{ex})$ as the height of the corresponding component.

Therefore, in the slow-exchange limit, the spectrum is given by three (two) lines with spacing between adjacent lines given by Eqs. (15a, 15b) having equal integrated intensities, equal line broadening, with heights given by Eqs. (11a, 11b) and (12), respectively.

It is worthwhile to reiterate that Disp_j is introduced into the absorption spectrum because of HSE and is detected as the out-of-phase component relative to the microwave field. We introduced the term "spin exchange-induced dispersion" [7], because its mathematical form is the same as the in-phase component of a Lorentzian absorption line. A spectrometer perfectly tuned to display only the absorption spectrum would give spectra shown in Figs. 1, 2, 3, 4, 5, 6, 7, 8 and 9 below. Often a small amount of the spectrum detected from the in-phase component is also present, a component that we have called instrumental dispersion. This component does not absorb energy, and unlike Disp_j, instrumental dispersion has the same sign for all three lines.

2.2 Intermediate Spin Exchange Case 1

Our hypothesis is that Eq. (1) is of the same form as Eq. (7), except that the variables $V_{ppj}(\omega_{ex})$, $H_j(\omega_{ex})$, $\Delta H_{ppj}(\omega_{ex})$, and $V_{dispj}(\omega_{ex})$ are not restricted to their perturbation values. Therefore, the spectrum is given by

$$Y = \sum_j \left(V_{ppj}(\omega_{ex}) \cdot \text{Abs}_j + V_{dispj}(\omega_{ex}) \cdot \text{Disp}_j\right), \tag{16}$$

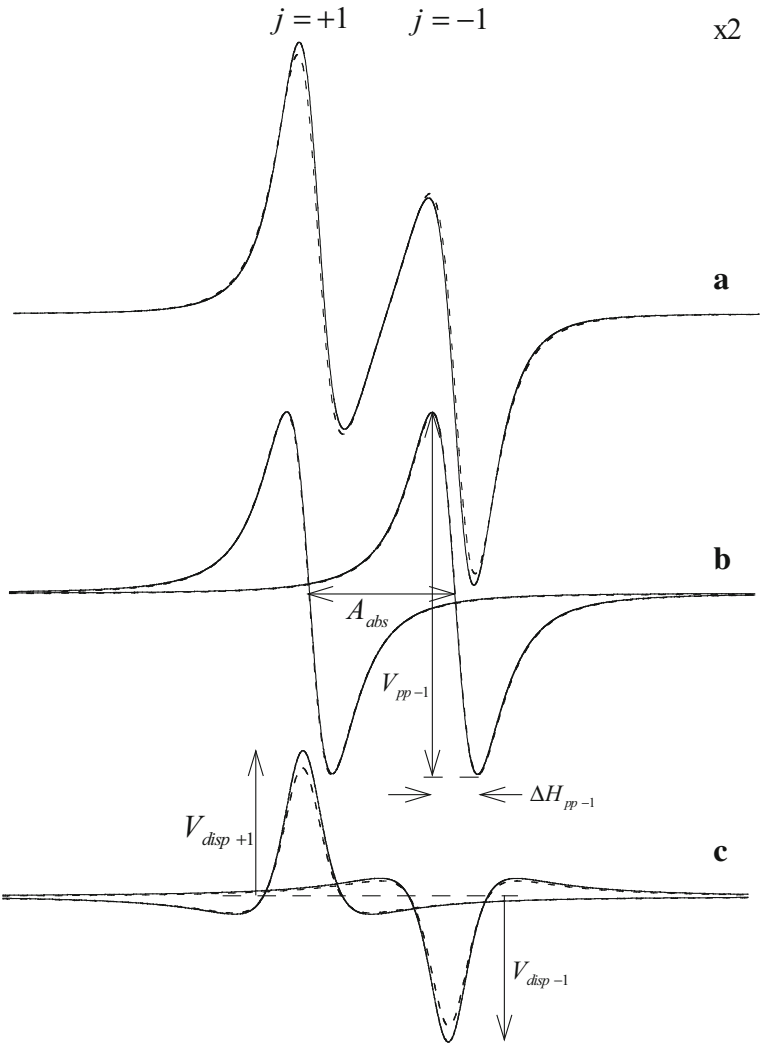

Fig. 1 **a** *Solid line* spectrum from Eq. (1); *dashed line* from perturbation theory, Eq. (16) for $\omega_{ex}/A_0\gamma = 0.463$. The maximum difference in the spectrum and the perturbation results is 9% of the maximum of the spectrum. **b** *Solid line* the absorption components as found from the fit of Eq. (16) to the spectrum in **a**; *dashed line* the perturbation results. **c** Dispersion components, *solid line* fit of Eq. (16) to the spectrum in part (**a**); *dashed line* the perturbation results. Fit parameters of Eq. (16) are indicated. The $\times 2$ is the relative scale of the ordinate applicable to Figs. 1, 2, 3, 4, 5, 6, 7, 8 and 9

with the same definitions Eqs. (4–6) except that the superscripts, pert, are removed. Of course, in the slow-exchange limit, Eq. (16) must reduce to Eq. (7). We justify our hypothesis by fitting Eq. (16) to Eq. (1).

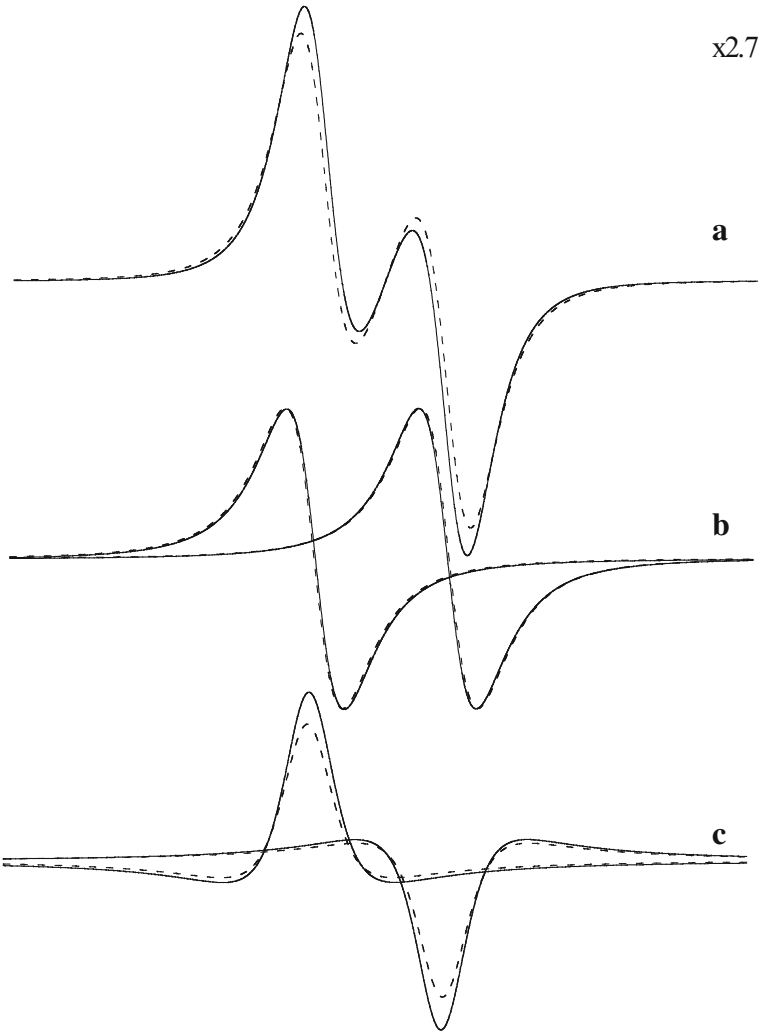

Fig. 2 Spectrum and various components as described in the caption to Fig. 1 for $\omega_{ex}/A_0\gamma = 0.590$

3 Methods

Equation (1) was computed using KaleidaGraph (2457 Perkiomen Ave, Reading, PA 19606) in double precision, which is accurate to 16 digits. Non-linear least-squares fits (fits) of Eq. (16) to spectra simulated by Eq. (1) were performed with the Levenberg–Marquardt algorithm in KaleidaGraph which finds the smallest value of the sum of the squared differences (χ^2) between the input data and the fit function. The algorithm was used without supplying expressions for the partial derivatives of the fit function with respect to the fit parameters. In this mode, the program finds numerical values of these derivatives beginning with first estimates of

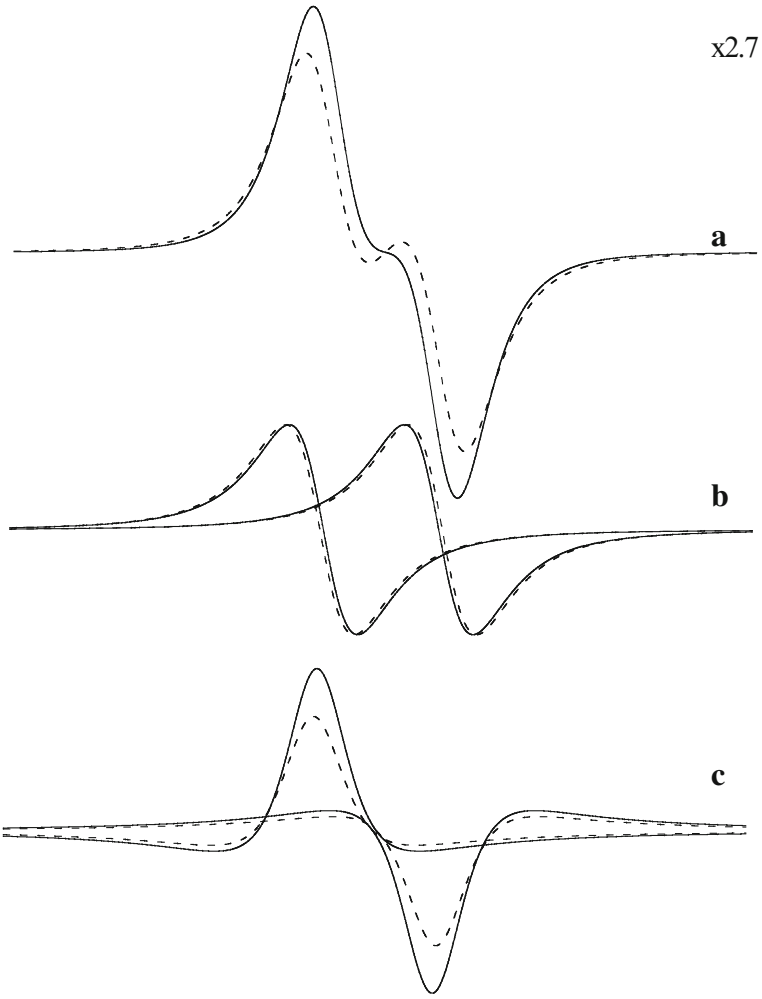

Fig. 3 Spectrum and various components as described in the caption to Fig. 1 for $\omega_{ex}/A_0\gamma = 0.709$

the parameters. The algorithm is accurate, efficient, and rapid provided that these estimates are reasonably close to the final values [10]. The values of the best-fit parameters are output with error estimates of the variables and χ^2. The program has a convenient feature that places the differences in the input points and the fit into a data window allowing the residuals to be easily plotted.

The bulk of the spectra were simulated with typical values [6] of $T_{2j}^{-1} = 0.2$ G and $A_0 = 22$ G for ^{15}N and to maintain a proper relationship with the known nuclear magnetic dipole moments [6], $A_0 = 22/1.403 = 15.681$ G for ^{14}N. All of the results are presented normalized to A_0; thus, they are available for any value of A_0. We began by simulating the spectra with 4096 points because we collect that many points experimentally, to be able to display residuals of the fits as high-resolution line graphs, and to accurately find line widths of spectra when they are

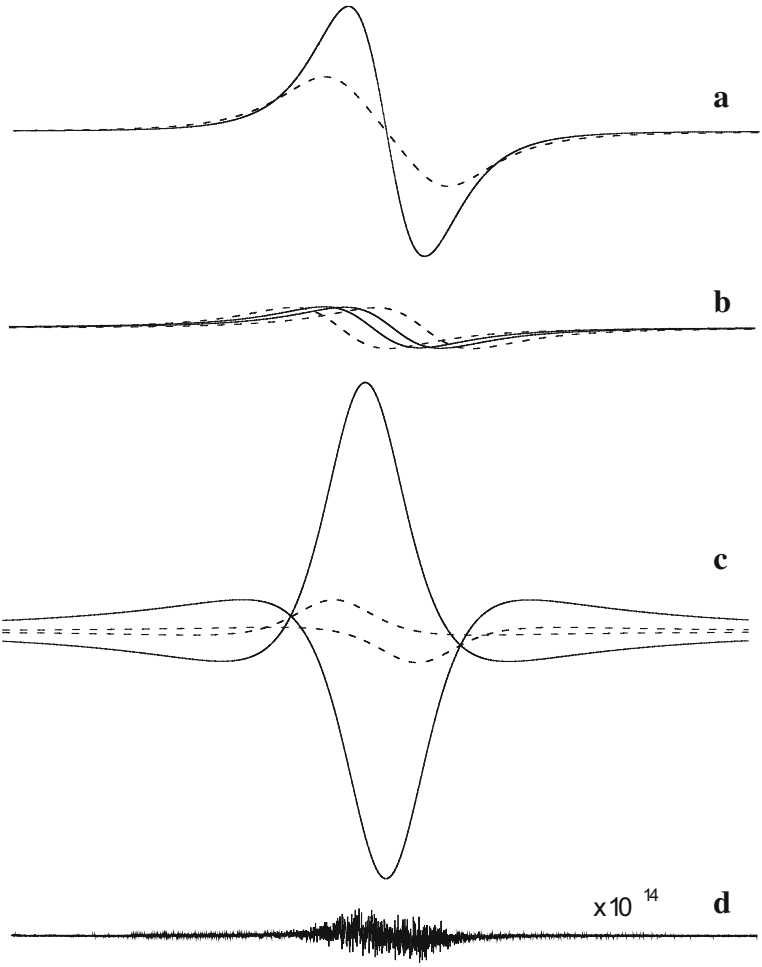

Fig. 4 Spectrum and various components as described in the caption to Fig. 1 for $\omega_{ex}/A_0\gamma = 0.992$. The absorption components, **b** appear deceptively small here because the scale of the ordinate is small and because the line width is large. The integrated intensity of the absorption components is the same in Figs. 1, 2, 3, 4 and 5. The difference between $A_{abs}(\omega_{ex})$ and $A_{abs}^{pert}(\omega_{ex})$, **b** is rather small until $\omega_{ex}/A_0\gamma$ approaches unity where it becomes more pronounced. The large difference in the exact and the perturbation results is in the dispersion component. **d** The residuals of the fit to Eq. (16) multiplied by 10^{14}

narrowed to one line. This many points is clearly an exaggeration for most purposes and may be reduced to as few as 26 with the same quality fits and identical results. To emphasize the details in the central parts of the spectra, Figs. 1, 2, 3, 4, 5, 6, 7, 8 and 9, are presented with 100-G magnetic field sweeps, not large enough to view the return to baseline for larger values of ω_{ex}. In fact, the fits and the parameters were verified to be independent of the sweep width by varying this parameter from 36 to 500 G.

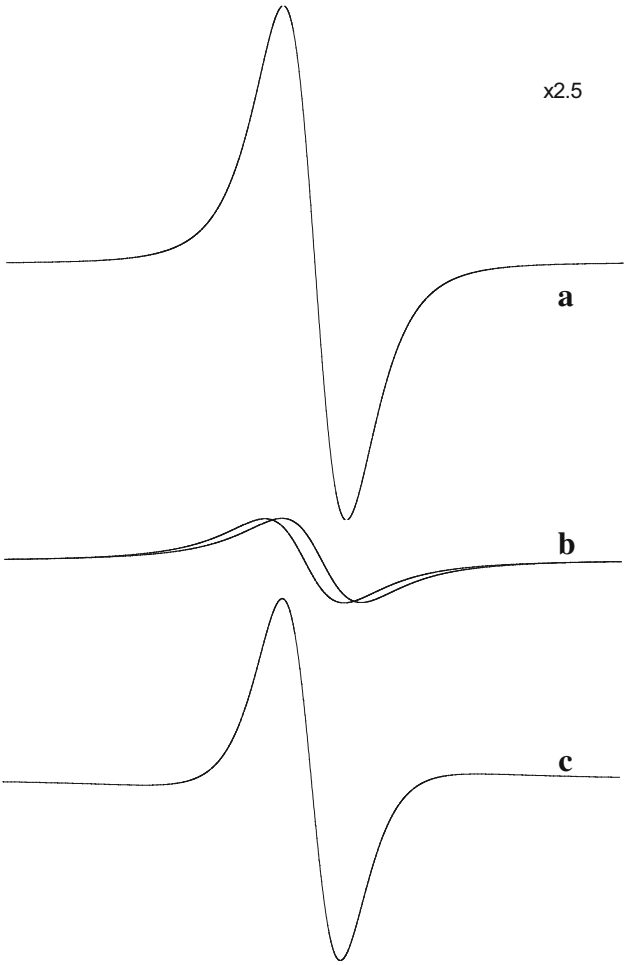

Fig. 5 Spectrum and components given in Fig. 4 except that **c** shows the sum of the two dispersion components and the scale has been increased by a factor of 2.5. This shows that a large fraction of the observed spectrum is provided by the dispersion components that, when summed, have the appearance of a single absorption line. Nevertheless, from Eq. (5), the summed dispersion lines have an integrated intensity of zero. The integrated intensity of the spectrum (**a**), is equal to that of the two absorption lines in **b**

All of the fits of Eq. (16) to Eq. (1) presented in this work resulted in a maximum discrepancy of less than 1×10^{-16}, the stated precision of KaleidaGraph in double precision. Therefore, all of the fits are limited only by the precision of the program. To avoid repetitive description of "fits limited only by the accuracy of the computer program", we searched for a short, properly descriptive adjective and settled on "perfect", obviously not in the literal meaning of the adjective. The estimated errors in the fit parameters were less than those given in Table 1, showing that the parameters are determined with extraordinary precision. We call two parameters "identical" if they are within the limits in Table 1. We say that a constant is

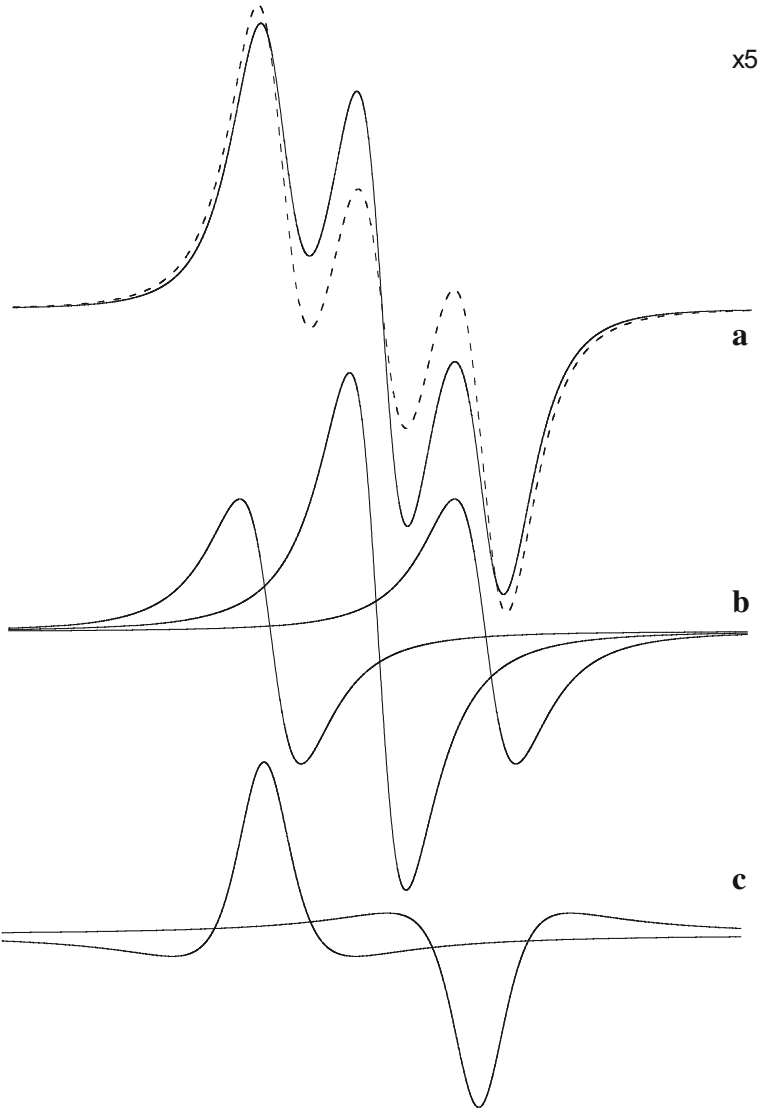

Fig. 6 Spectrum and various components of an ^{14}N nitroxide for $\omega_{ex}/A_0\gamma = 0.649$. The significance of the lines is described in the caption to Fig. 1; however, A_0 is the spacing between adjacent lines. Perturbation results are not presented for the individual components to simplify Figs. 6, 7, 8 and 9. The dramatic differences in the heights of the absorption components show that they are very different than their perturbation counterparts, where all three lines are of equal height and line width

"exact", if it is to within ±1 in the 16th digit. Our intention, here, is not to provide ridiculously accurate results, but rather to make the case that Eqs. (1) and (16) are the same within the accuracy of the computer program. It is rather remarkable that the parameters can be recovered to accuracies better than Table 1, because the

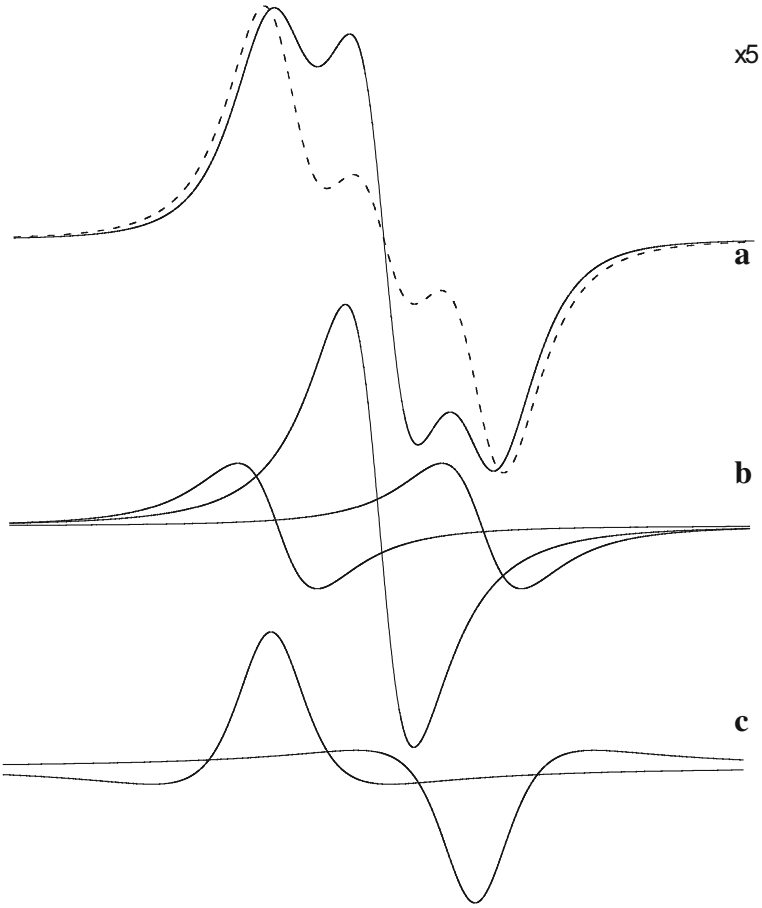

Fig. 7 Spectrum and various components of an ^{14}N nitroxide for $\omega_{ex}/A_0\gamma = 0.828$

functions in Eq. (16) are not orthogonal even in the slow-exchange limit and not even remotely so for $\omega_{ex}/\gamma \approx A_0$.

To fit Eq. (16) to Eq. (1) for ^{15}N, there are potentially eight variables; however, because of the symmetry of V_{ppj} and $\Delta H_{ppj}(\omega_{ex})$ and the anti-symmetry of V_{dispj} and δH_j, only four are independent. For ^{14}N, there are potentially 12 variables, but because of the same symmetry arguments and the facts that the center line is neither shifted nor has a dispersion component [3, 7], the number of independent variables is reduced to 6. Preliminary work allowed all parameters to vary freely showing that $V_{pp+1}(\omega_{ex}) = V_{pp-1}(\omega_{ex})$, $B_{+1} = B_{-1}$, $V_{disp+1}(\omega_{ex}) = -V_{disp-1}(\omega_{ex})$ and $\delta H_{+1} = -\delta H_{-1}$ to 16 digits as expected. The bulk of the work used these symmetry properties to reduce the number of fit variables and to simplify the tables.

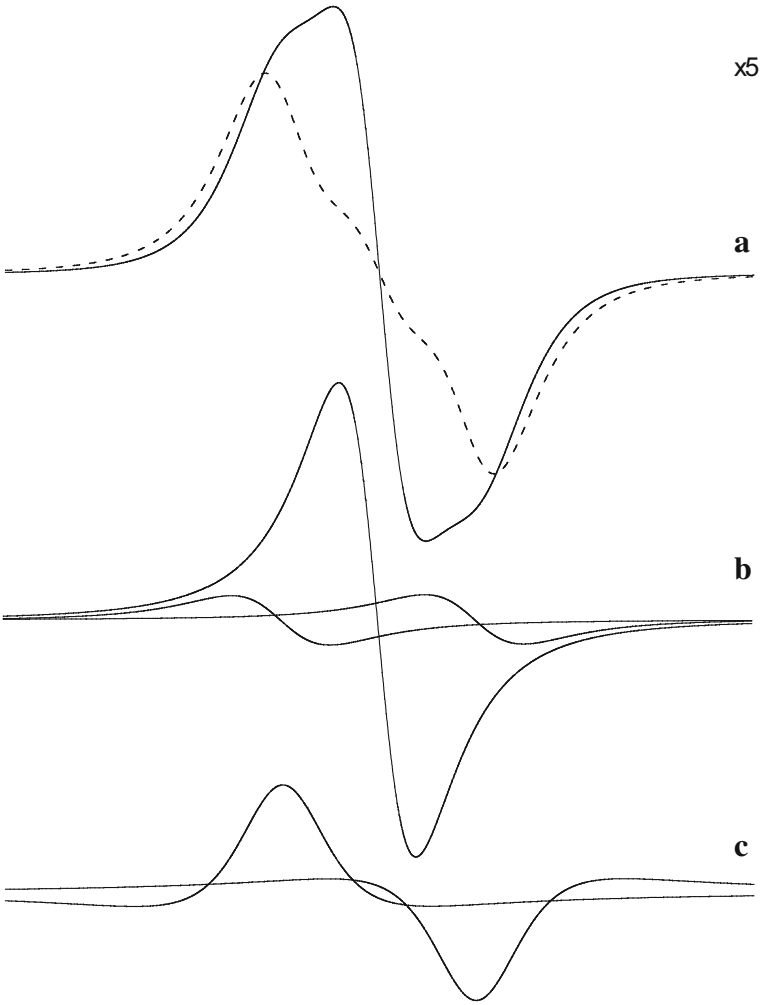

Fig. 8 Spectrum and various components of an ^{14}N nitroxide for $\omega_{ex}/A_0\gamma = 0.994$

4 Results

4.1 ^{15}N Nitroxides

Figures for slow exchange are not presented because these have been published and are known to adhere to the perturbation results [6–8]. The figures are all presented with a 100-G sweep with the magnetic field increasing from left to right. All of the spectra were simulated with the same arbitrary value of I_{total} so that the spectrum and component heights maintain their correct relative values throughout the paper. For clarity, the relative scales of the ordinates in Figs. 1, 2, 3, 4, 5, 6, 7, 8 and 9 are adjusted as indicated in the upper right-hand corner of the figures. Note that these relative

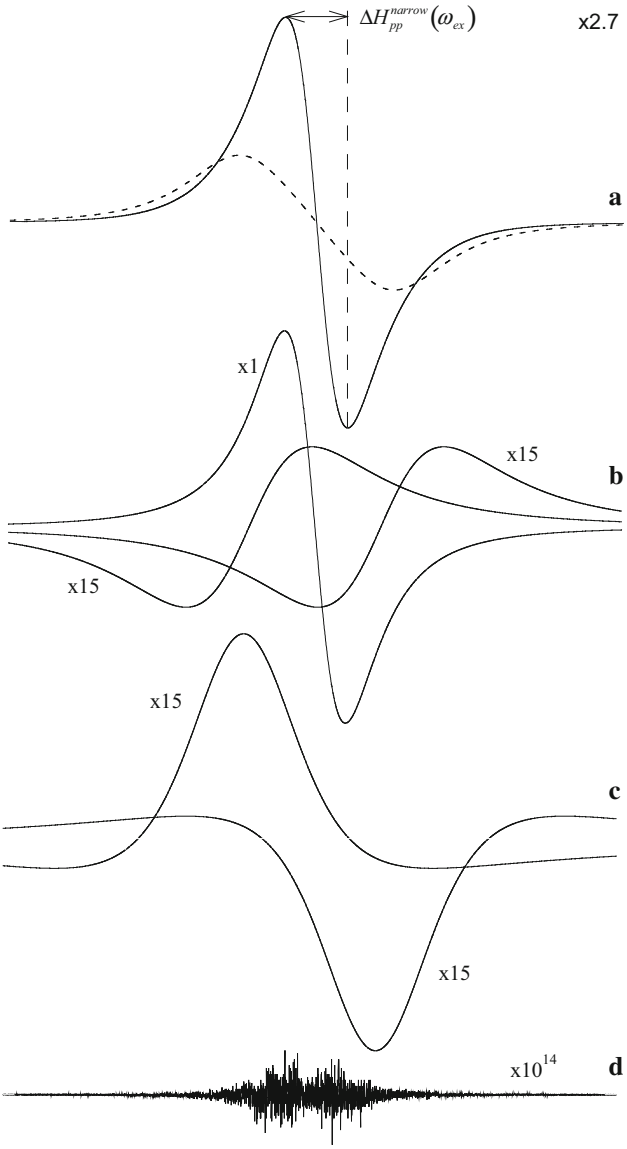

Fig. 9 **a–c** Spectrum and various components of an ^{14}N nitroxide for $\omega_{ex}/A_0\gamma = 1.39$. **d** The difference in the sum of the components and the spectrum multiplied by 10^{14}. The residuals here appear to be larger than those for ^{15}N, Fig. 4b; however, the scale of this spectrum is 2.7 times larger. The dispersion and the two outer absorption components are too small to be perceived on the same scale as the spectrum; so, they are amplified by a factor of 15 revealing the fact that the two outer absorption components are negative and, thus, have negative integrated intensities. Nevertheless, the sum of the intensities of the central line, $I_0/I_{total} = 1.30620$, and the two outer lines, $2I_{\pm1}/I_{total} = -0.30620$, add to exactly unity

Table 1 Maximum estimated errors in the variables

	δH_j	$V_{pp\pm1}$	V_{pp0}	$\Delta H_{pp\pm1}$	ΔH_{pp0}	$\pm V_{disp\pm1}$
^{14}N	4×10^{-13}	6×10^{-18}	1×10^{-17}	2×10^{-13}	2×10^{-15}	3×10^{-17}
^{15}N	4×10^{-15}	4×10^{-18}	–	3×10^{-15}	–	1×10^{-16}

heights would correspond to constant-concentration experiments in which ω_{ex} were varied by varying the temperature and/or the viscosity. For a constant-temperature experiment, the heights would be multiplied by a factor proportional to ω_{ex}.

The solid line in the first trace of Figs. 1, 2, 3, 4, 5, 6, 7, 8 and 9 is computed from Eq. (1).

Figures 1a, 2, 3 and 4a show representative spectra for ^{15}N (solid lines) given by Eq. (1) at increasing values of $\omega_{ex}/A_0\gamma = 0.463$, 0.590, 0.709, and 0.992, respectively. The dashed lines are the perturbation results, Eq. (7). The maximum difference in the spectrum and perturbation result in Fig. 1a is 9.4% of the maximum of the spectrum. This discrepancy becomes more severe as $\omega_{ex}/A_0\gamma$ increases.

Figures 1b, 2, 3 and 4b show the absorption components derived from fits of Eq. 16 to Eq. (1) and Figs. 1c, 2, 3 and 4c, the dispersion components. In Fig. 1b, c, the parameters $\Delta H_{pp-1}(\omega_{ex})$, A_{abs}, V_{pp-1}, and $V_{disp\pm1}$ are indicated. The resonance fields are where the absorption components cross the baseline, or where the dispersion components reach their extremum values.

As $\omega_{ex}/A_0\gamma$ increases, there is only a slight difference in the correct and perturbation values of the resonance fields, Figs. 1b, 2 and 3b, until near the point where the two-line pattern collapses completely, Fig. 4b. Values of $V_{pp\pm1}$ and $\Delta H_{pp\pm1}$ of the correct spectra and the perturbation components are identical for all values of ω_{ex}. For the dispersion components, significant differences in the values of $V_{disp\pm1}$ and $V_{disp\pm1}^{pert}$ are observed already in Fig. 1c becoming more significant until $Disp_{\pm1}$ dominates the spectrum in Fig. 4. Figure 4, at a relative scale = 1, is deceptive because of this dominance. The absorption components appear to be insignificant when, in fact, their integrated intensities are identical to those in Figs. 1, 2 and 3. Figure 4d displays the difference in the sum of the components and the spectrum multiplied by 10^{14}. The maximum value of the residuals is 3.6×10^{-17}, less than the stated accuracy of KaleidaGraph.

It is instructive to present the results in Fig. 4 as Fig. 5 where, in (c), instead of the separate dispersion components, we plot the sum of the two. Figure 5 is plotted on a scale 2.5 times larger than that of Fig. 4; thus, the two rather dominant dispersion lines now have the appearance of a much smaller absorption line that, nevertheless, provides a major portion of the spectrum. Note that despite the appearance of part c, it contributes nothing to the integrated intensity, as shown by Eq. (5) where the even function, integrated twice, gives zero.

We have managed to find perfect fits only up to $\omega_{ex}/A_0\gamma = 0.99908$ and it is easy to appreciate why from Fig. 4. As the dispersion lines move closer together and grow larger, a very minor error in providing the first estimate in either the position or dispersion maximum value results in an unstable minimum in parameter space.

Indeed, at zero spacing, $\pm V_{\text{disp}\pm1}$ could be any arbitrary value because the two would cancel. Providing first estimates is rather easy up to approximately $\omega_{\text{ex}}/A_0\gamma = 0.9$; above this, more patience and perseverance is needed. One can get splendid fits to the spectra but not perfect fits; $\chi^2 \sim 10^{-12}$ rather than $\chi^2 \sim 10^{-32}$ with identical parameters but these are not included in the present paper.

Table 2 tabulates the fitted parameters for ^{15}N and Table 3 presents the perturbation results as well as the important parameter $\pm V_{\text{disp}\pm1}/V_{\text{pp}\pm1}$ [1, 6–8, 11–13]. All entries given as fractions In Tables 2, 3, 4 and 5 are exact to within ±1 in the least-significant of 16 digits. Comparing Tables 2 and 3 highlights the fact that values of $V_{\text{pp}\pm1}$ and $\Delta H_{\text{pp}\pm1}$ are identical for the absorption components and their perturbation counterparts, but only to five significant figures; in fact, the largest difference is 5×10^{-16}. Only $\pm V_{\text{disp}\pm1}/V_{\text{pp}\pm1}$ and A_{abs}/A_0 depart from the perturbation predictions. We have failed in our efforts to find expressions for $\pm V_{\text{disp}\pm1}/V_{\text{pp}\pm1}$ or A_{abs}/A_0; however, it is very interesting that the product of the two is very simple as follows:

$$\frac{A_{\text{abs}}(\omega_{\text{ex}})}{A_0}\frac{V_{\text{disp}\pm1}}{V_{\text{pp}\pm1}} = \frac{4}{3\sqrt{3}}\frac{\omega_{\text{ex}}}{\gamma A_0}, \tag{17}$$

Table 2 Fit parameters ^{15}N spectra

$\omega_{\text{ex}}/\gamma A_0$	$B_{\pm1}/A_0$ [a]	$V_{\text{pp}\pm1}/I_{\text{total}}$	$\pm V_{\text{disp}\pm1}/I_{\text{total}}$ [b]	A_{abs}/A_0
0.15746	0.090909	0.17400	0.021358	0.98753
0.31492	0.18182	0.048379	0.012357	0.94912
0.46293	0.26727	0.023191	0.0093235	0.88639
0.59047	0.34091	0.014490	0.0081609	0.80706
0.70857	0.40909	0.010163	0.0078562	0.70564
0.78730	0.45455	0.0082737	0.0081326	0.61658
$\sqrt{3}/2$	1/2	0.0068659	0.0091546	1/2
0.90460	0.52227	0.0063038	0.010298	0.42626
0.94475	0.54545	0.0057891	0.012845	0.32778
0.96208	0.55545	0.0055863	0.015167	0.27278
0.97703	0.56409	0.0054197	0.019130	0.21308
0.98569	0.56909	0.0053266	0.023980	0.16854
0.99199	0.57273	0.0052603	0.031806	0.12629
0.99593	0.57500	0.0052196	0.044395	0.090139
0.99672	0.57545	0.0052115	0.049384	0.080970
0.99750	0.57591	0.0052034	0.056585	0.070613
0.99829	0.57636	0.0051954	0.068322	0.058437
0.99908	0.57682	0.0051873	0.092947	0.042923

Dependences on $\omega_{\text{ex}}/\gamma A_0$ are suppressed in the headings. All entries given as fractions are exact to within ±1 in the least-significant of 16 digits

[a] Identical to $B_{\pm1}^{\text{pert}}/A_0$, Eq. (9a)

[b] Identical to $\pm V_{\text{disp}\pm1}^{\text{pert}}/I_{\text{total}}$, Eq. (11b)

Table 3 Perturbation values ^{15}N spectra and values of $\pm V_{\mathrm{disp}\pm1}/V_{\mathrm{pp}\pm1}$

$\omega_{\mathrm{ex}}/\gamma A_0$	$B^{\mathrm{pert}}_{\pm1}/A_0$	$\pm V^{\mathrm{pert}}_{\mathrm{disp}\pm1}/V^{\mathrm{pert}\ a}_{\mathrm{pp}\pm1}$	$\pm V_{\mathrm{disp}\pm1}/V_{\mathrm{pp}\pm1}$	$A^{\mathrm{pert}}_{\mathrm{abs}}/A_0$ [b]
0.15746	0.090909	0.12121	0.12274	0.98760
0.31492	0.18182	0.24242	0.25542	0.95041
0.46293	0.26727	0.35636	0.40204	0.89285
0.59047	0.34091	0.45455	0.56321	0.82567
0.70857	0.40909	0.54545	0.77299	0.74897
0.78730	0.45455	0.60606	0.98295	0.69008
$\sqrt{3}/2$	1/2	2/3	4/3	5/8
0.90460	0.52227	0.69636	1.6337	0.59085
0.94475	0.54545	0.72727	2.2188	0.55372
0.96208	0.55545	0.74061	2.7150	0.53721
0.97703	0.56409	0.75212	3.5297	0.52270
0.98569	0.56909	0.75879	4.5021	0.51420
0.99199	0.57273	0.76364	6.0465	0.50798
0.99593	0.57500	0.76667	8.5054	0.50406
0.99672	0.57545	0.76727	9.4760	0.50328
0.99750	0.57591	0.76788	10.875	0.50249
0.99829	0.57636	0.76848	13.151	0.50171
0.99908	0.57682	0.76909	17.918	0.50092

Dependences on $\omega_{\mathrm{ex}}/\gamma A_0$ are suppressed in the headings. All entries given as fractions are exact to within ±1 in the least-significant of 16 digits

[b] Equations (11b) and (12)

[c] Equation (15b)

Forming this product from the data in Tables 2 and 3, shows that the two sides of Eq. (17) are equal to within 2×10^{-7}–5×10^{-5}; however, this is because of round-off error due to using only five significant figures. With data of full precision, the two sides are the same to within 6×10^{-15}.

Table 2 shows that, the case of ^{15}N, Eq. (1) yields simple results for $\omega_{\mathrm{ex}}/A_0\gamma = \sqrt{3}/2$, where $B_{\pm1} = A_0/2$ and $A_{\mathrm{abs}} = A_0/2$, or $B_{\pm1} = A_{\mathrm{abs}}$. Table 4 shows that the perturbation results are also simple at $\omega_{ex}/A_0\gamma = \sqrt{3}/2$ where $A^{\mathrm{pert}}_{\mathrm{abs}} = 5A_0/8$. Furthermore, we see that $\pm V_{\mathrm{disp}\pm1}/V_{\mathrm{pp}\pm1} = 2\ \pm V^{\mathrm{pert}}_{\mathrm{disp}\pm1}/V^{\mathrm{pert}}_{\mathrm{pp}\pm1}$.

4.2 ^{14}N Nitroxides

Figures 6a, 7, 8 and 9a show representative results for ^{14}N at increasing values of $\omega_{\mathrm{ex}}/A_0\gamma = 0.649$, 0.828, 0.994, and 1.39, respectively. The significance of the lines is described in the caption to Fig. 1; however, A_0 is the spacing between adjacent lines, not the outer lines. For clarity, the perturbation results are not presented for the components, only for the spectra. As $\omega_{\mathrm{ex}}/A_0\gamma$ increases, the components broaden and move toward the center, while the spectra coalesce into one line and narrow. The dramatic differences in the heights of the absorption components show

Table 4 Fit parameters ^{14}N spectra

$\omega_{ex}/\gamma A_0$	$B_{\pm1}/A_0$	B_0/A_0	$V_{pp\pm1}/I_{total}$	V_{pp0}/I_{total}	$\pm V_{disp\pm1}/I_{total}$	A_{abs}/A_0
0.16568	0.12774	0.12715	0.11461	0.11881	0.014822	0.99541
0.33137	0.25670	0.25186	0.030629	0.035613	0.0082785	0.98153
0.49705	0.38835	0.37118	0.013077	0.018764	0.0057557	0.95798
0.64952	0.51364	0.47276	0.0068868	0.013460	0.0044905	0.92724
0.66273	0.52474	0.48103	0.0065294	0.013197	0.0044052	0.92416
0.82842	0.66912	0.57490	0.0032585	0.011494	0.0035148	0.87947
0.99410	0.82686	0.64204	0.0012666	0.012170	0.0027721	0.82409
$2/\sqrt{3}$	1.0000	2/3	3×10^{-16}	0.015171	0.0019904	0.76376
1.1598	1.0059	0.66664	-3×10^{-5}	0.015306	0.0019636	0.76184
1.3255	1.2107	0.63959	−0.000596	0.020631	0.0010980	0.70422
1.3917	1.2980	0.61797	−0.000626	0.022984	0.00081433	0.68557
1.4083	1.3202	0.61202	−0.000622	0.023573	0.00075275	0.68137
1.4911	1.4315	0.58076	−0.000561	0.026483	0.00050334	0.66313
3/2	$5\sqrt{3}/6$	$\sqrt{3}/3$	−0.000552	0.026791	0.00048199	0.66144
1.5740	1.5429	0.54911	−0.000472	0.029366	0.00033663	0.64893
1.6568	1.6537	0.51890	−0.000386	0.032278	0.00022863	0.63789
1.6983	1.7087	0.50461	−0.000347	0.033761	0.00018994	0.63331
1.7397	1.7633	0.49091	−0.000312	0.035268	0.00015212	0.62925
1.8225	1.8718	0.46532	−0.000253	0.038366	0.00010768	0.62238
1.9054	1.9791	0.44204	−0.000205	0.041589	7.7971e−05	0.61685
1.9882	2.0853	0.42089	−0.000168	0.044944	5.7655e−05	0.61233

Dependences on $\omega_{ex}/\gamma A_0$ are suppressed in the headings. All entries given as fractions are exact to within ±1 in the least-significant of 16 digits

that they are very different than their perturbation counterparts, where all three lines are of equal height and line width.

For $\omega_{ex}/A_0\gamma = 1.39$, Fig. 9, both the outer absorption lines and the dispersion lines are barely perceptible, so they are amplified by a factor of 15 relative to the spectrum and the central absorption component. Figure 9d shows the residuals of the fit amplified by 10^{14}. The maximum value of the residue is 2.5×10^{-17}, similar to that in Fig. 4d. Figure 9b shows a feature that is extremely interesting and, to our knowledge, unprecedented: $V_{pp\pm1} < 0$. As in the case of ^{15}N, the sum of the two dispersion components (not shown) appears to be a smaller single line with the appearance of an absorption line; however, for ^{14}N, it contributes much less to the spectrum.

We have managed to find perfect fits up to $\omega_{ex}/A_0\gamma = 1.9882$, about twice the upper limit of 0.99908 for ^{15}N. For convenience, call these upper limits $(\omega_{ex}/\gamma A_0)_{upper}$; however, we do not mean to imply that fits above these limits are not possible.

Table 4 tabulates the fitted parameters for ^{14}N and Table 5 presents the perturbation results, the integrated intensities, and the important parameter

Table 5 Perturbation values ^{14}N spectra, integrated intensities, and values of $\pm V_{\mathrm{disp}\pm1}/V_{\mathrm{pp}\pm1}$

$\omega_{\mathrm{ex}}/\gamma A_0$	B^{pert}/A_0 [a]	$I_{\pm1}/I_{\mathrm{total}}$	I_0/I_{total}	$V^{\mathrm{pert}}_{\mathrm{disp}\pm1}/V^{\mathrm{pert}}_{\mathrm{pp}\pm1}$ [b]	$V_{\mathrm{disp}\pm1}/V_{\mathrm{pp}\pm1}$	$A^{\mathrm{pert}}_{\mathrm{abs}}/A_0$ [b]
0.16568	0.12754	0.33024	0.33953	0.12754	0.12933	0.99542
0.33137	0.25509	0.32035	0.35930	0.25509	0.27029	0.98170
0.49705	0.38263	0.30164	0.39672	0.38263	0.44012	0.95882
0.64952	0.50000	0.27295	0.45411	0.50000	0.65204	0.92969
0.66273	0.51017	0.26977	0.46046	0.51017	0.67467	0.92680
0.82842	0.63771	0.21633	0.56733	0.63771	1.0786	0.88562
0.99410	0.76526	0.12736	0.74529	0.76526	2.1887	0.83529
$2/\sqrt{3}$	8/9	0.00000[c]	1.0000	8/9	∞[d]	7/9
1.1598	0.89280	−0.00440	1.0088	0.89280	−65.998	0.77582
1.3255	1.0203	−0.12698	1.2540	1.0203	−1.8435	0.70719
1.3917	1.0714	−0.15310	1.3062	1.0714	−1.3013	0.67718
1.4083	1.0841	−0.15728	1.3146	1.0841	−1.2107	0.66945
1.4911	1.1479	−0.16660	1.3332	1.1479	−0.89708	0.62941
3/2	$2/\sqrt{3}$	−1/6	4/3	$2/\sqrt{3}$	−0.87287	5/8
1.5740	1.2117	−0.16269	1.3254	1.2117	−0.71273	0.58709
1.6568	1.2754	−0.15245	1.3049	1.2754	−0.59264	0.54249
1.6983	1.3073	−0.14636	1.2927	1.3073	−0.54722	0.51932
1.7397	1.3392	−0.14006	1.2801	1.3392	−0.48751	0.49559
1.8225	1.4030	−0.12758	1.2552	1.4030	−0.42643	0.44641
1.9054	1.4667	−0.11593	1.2319	1.4667	−0.37959	0.39494
1.9882	1.5305	−0.10540	1.2108	1.5305	−0.34250	0.34118

Dependences on $\omega_{\mathrm{ex}}/\gamma A_0$ are suppressed in the headings. All entries given as fractions are exact to within ±1 in the least-significant of 16 digits

[a] Equation (9a). Average broadening, $(B_0 + 2B_{\pm1})/3A_0$ is identical to B^{pert}/A_0

[b] Equation (15a)

[c] 4×10^{-14}

[d] 7×10^{12}

$\pm V_{\mathrm{disp}\pm1}/V_{\mathrm{pp}\pm1}$ [1, 6–8, 11–13]. Here, the results are far more interesting than for ^{15}N, because there are differences between the exact and perturbation results for every parameter. We have not been able to find any simple relationships between the exact and perturbation results similar to that in Eq. (17).

Tables 4 and 5 show that, in the case of ^{14}N, Eq. (1) yields simple results for two values of $\omega_{\mathrm{ex}}/A_0\gamma$.

At $\omega_{\mathrm{ex}}/A_0\gamma = 2/\sqrt{3}$,

1. $B_{\pm1} = A_0$ and $B_{\pm1} = 2A_0/3$, its maximum value, while $B_j^{\mathrm{pert}} = 8A_0/9$.
2. $I_{\pm1}/I_{\mathrm{total}} = 0$, above which it is negative, and
3. $A^{\mathrm{pert}}_{\mathrm{abs}} = 7A_0/9$ while $A_{\mathrm{abs}} = 0.76376A_0$.

At $\omega_{\mathrm{ex}}/A_0\gamma = 3/2$,

1. $B_{\pm1} = \left(5\sqrt{3}/6\right)A_0$ and $B_0 = \left(\sqrt{3}/3\right)A_0$, while $B_j^{\mathrm{pert}} = 5A_0/8$.

Fig. 10 **a** Normalized broadening ^{14}N: *outer lines*, *squares center line*, *crosses* average from Eq. (18),▶ *circles* and perturbation theory, *straight line*. **b** Normalized broadening ^{15}N, *circles* perturbation theory *straight line*. *Solid diamonds* in both **a**, **b**, net normalized line width of the narrowed spectra, $\left[\Delta H_{\mathrm{pp}}^{\mathrm{narrow}}(\omega_{\mathrm{ex}}) - \Delta H_{\mathrm{pp}}(0)\right]/A_0$, where $\Delta H_{\mathrm{pp}}^{\mathrm{narrow}}(\omega_{\mathrm{ex}})$ is the peak-to-peak line width of the narrowed line measured directly from the spectra (see Fig. 9a)

2. $I_{\pm1}/I_{\mathrm{total}} = -1/6$, its minimum value, and $I_0/I_{\mathrm{total}} = 4/3$, its maximum, and
3. $A_{\mathrm{abs}}^{\mathrm{pert}} = 5A_0/8$ while $A_{\mathrm{abs}} = 0.66144A_0$.

We do not recognize the numbers 0.76376 or 0.66144, but their ratio 0.76376/0.66144 $= 2/\sqrt{3}$ to 8 digits.

For ^{14}N, Fig. 10a displays the differential line broadening of the outer lines, squares, and the center line, crosses. The solid diamonds are values of $\left[\Delta H_{\mathrm{pp}}^{\mathrm{narrow}}(\omega_{\mathrm{ex}}) - \Delta H_{\mathrm{pp}}(0)\right]/A_0$, where $\Delta H_{\mathrm{pp}}^{\mathrm{narrow}}(\omega_{\mathrm{ex}})$ is the peak-to-peak line width of the narrowed line measured directly from the spectrum, Fig. 9a. The outer lines continue to broaden up to $(\omega_{\mathrm{ex}}/\gamma A)_{\mathrm{upper}}$; however, in contrast, the central line width reaches a maximum value of $(2A_0/3)$ at exactly $(\omega_{\mathrm{ex}}/A_0\gamma) = 2/\sqrt{3}$ and then decreases. Therefore, the observed line width of the collapsed spectrum decreases while the average line width of the components continues to increase linearly with $(\omega_{\mathrm{ex}}/\gamma A_0)$. Values of $\Delta H_{\mathrm{pp}}^{\mathrm{narrow}}$ are dominated by ΔH_{pp0} because of the reduced height of the outer lines; compare the crosses with the diamonds. The straight line is the perturbation prediction and the circles are the averages computed from:

$$\langle B \rangle = (2B_{\pm1} + B_0)/3 \text{ For}^{14}\text{N} \tag{18}$$

From columns 2 and 3 of Table 4, we find that average value of the broadening is exactly equal to the perturbation value, column 2 of Table 5.

Figure 10b, circles, displays the broadening of ^{15}N; the straight line is the perturbation prediction. The solid diamonds are as described in (a). The lines continue to broaden linearly with $\omega_{\mathrm{ex}}/A_0\gamma$ up to $(\omega_{\mathrm{ex}}/\gamma A)_{\mathrm{upper}}$, but $\Delta H_{\mathrm{pp}}^{\mathrm{narrow}}(\omega_{\mathrm{ex}})$ begins to decrease before that.

Figure 11 shows twice the integrated intensity of each of the outer lines, squares, and the intensity of the central line, crosses. The two outer lines yield 2/3 of the total intensity at small $\omega_{\mathrm{ex}}/A_0\gamma$ and the center gives 1/3 as predicted by perturbation theory. From columns 3 and 4 of Table 5, we find that the average integrated intensity is exactly equal to I_{total}

$$\sum_j I_j = (2I_{\pm1} + I_0) = I_{\mathrm{total}} \text{ For } ^{14}\text{N}, \tag{19}$$

even for the range of $\omega_{\mathrm{ex}}/A_0\gamma > 2/\sqrt{3}$ where $I_{\pm1} < 0$ because $I_0 > I_{\mathrm{total}}$. The intensity of the outer lines is zero at $\omega_{ex}/A_0\gamma = 2/\sqrt{3}$; thus, $I_0 = 3I^{\mathrm{pert}} = I_{\mathrm{total}}$ at that point. The resulting spectrum at that point consists of one absorption line plus two rather small dispersion lines, similar to Fig. 9 but without the outer absorption lines. The intensity is equally shared by the central and outer lines, respectively; i.e., the intensity of the central line is equal to twice the intensity of each of the outer lines, at $\omega_{\mathrm{ex}}/\gamma A_0 = 0.7344$. The straight horizontal line at unity is the perturbation result and the circles are the averages.

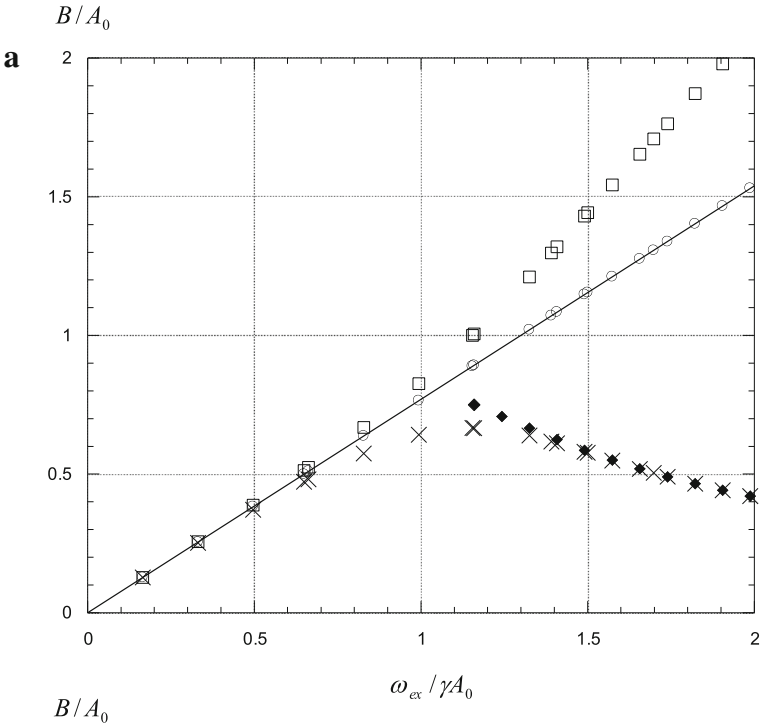
a
B/A_0
2
1.5
1
0.5
0
0
0.5
1
1.5
2
$\omega_{ex}/\gamma A_0$

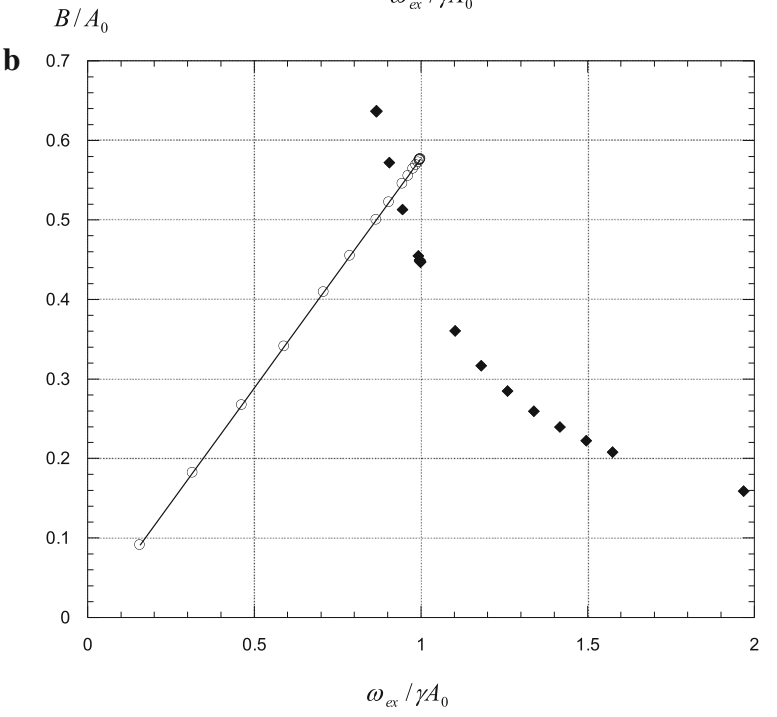
b
B/A_0
0.7
0.6
0.5
0.4
0.3
0.2
0.1
0
0
0.5
1
1.5
2
$\omega_{ex}/\gamma A_0$

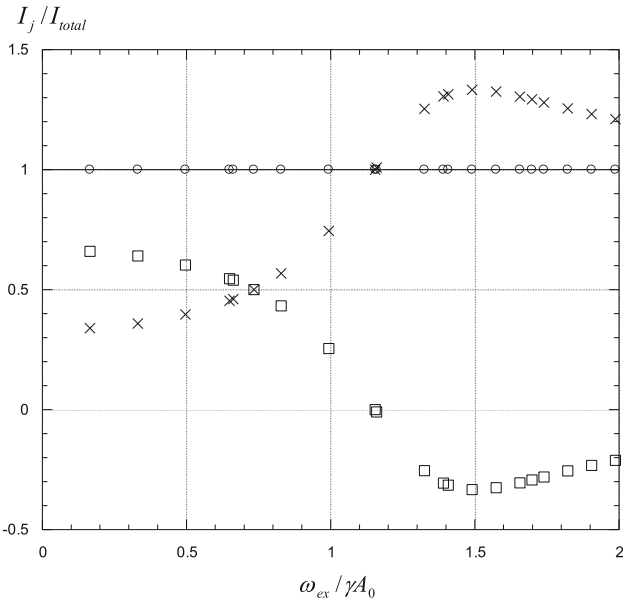

Fig. 11 ^{14}N integrated intensity of the *center line*, *crosses*, twice the intensity of the *outer lines*, *squares*, average intensity, Eq. (19), *circles*, and perturbation theory, *straight horizontal line* at unity

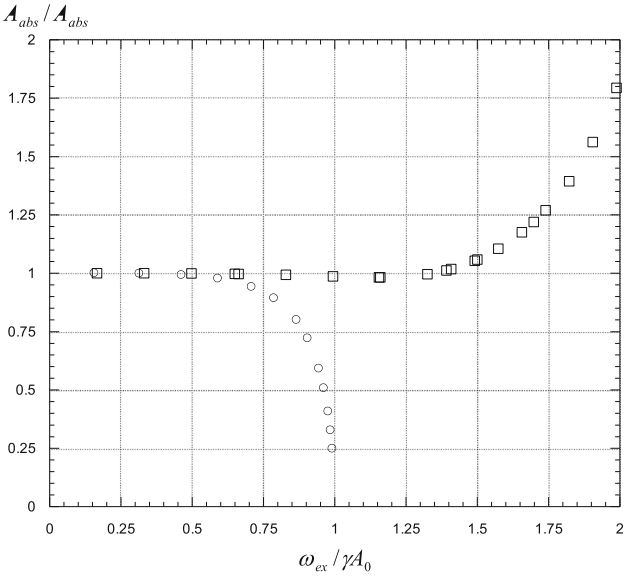

Fig. 12 Departure of line shifts from the perturbation predictions for ^{14}N *squares*, and ^{15}N *circles*

Figure 12 shows the dramatic difference in the line shifts for ^{15}N and ^{14}N. For both isotopes, the outer lines shift toward the center slightly faster than the perturbation prediction at small values of $\omega_{\mathrm{ex}}/A_0\gamma$, but the discrepancy is rather

small for both isotopes until well into the intermediate HSE region. For ^{15}N, the discrepancy in the shifts is less than 1% up to $\omega_{ex}/\gamma A_0 = 0.500$, above which the discrepancy increases rapidly. For ^{14}N, the discrepancy is less than 1% up to $\omega_{ex}/\gamma A_0 = 0.910$, and reaches a maximum of 1.8% near $\omega_{ex}/A_0\gamma = 2/\sqrt{3}$. Near $\omega_{ex}/A_0\gamma = 4/3$, the discrepancy is zero, increasing to 1% at $\omega_{ex}/A_0\gamma = 1.38$, after which, it increases rapidly, but in the opposite sense as that of ^{15}N.

5 Discussion

5.1 Line Broadening in Hyperfine Multiplets

The two cases that we have treated here show that the average broadening is equal to the perturbation prediction, Eqs. (9a, 9b), trivially for ^{15}N and by direct computation for ^{14}N up to $(\omega_{ex}/A_0\gamma)_{upper}$.

In Ref. [9], Eq. (1) was used to simulate five-line spectra to study a nitrone. In that case, the situation was more interesting because ρ_j = 1/9:2/9:3/9:2/9:1/9 rather than equal statistical factors of 1/2 or 1/3 for ^{15}N or ^{14}N, respectively. The factors in Eqs. (9a, 9b) vary as 8/9:7/9:6/9:7/9:8/9 from line 1 to 5. That case was treated only up to $\omega_{ex}/A_0\gamma = 0.487$; thus, the very interesting phenomenon of negative absorption intensities was not discovered, if, indeed, it exists in the five-line case. Differential line broadening and integrated intensities were quite evident as demonstrated in Figs. 5 and 7 of Ref. [9], but in common with ^{15}N and ^{14}N, the average broadenings and average intensities were equal to the perturbation predictions. In summary, for two-, three-, and five-line multiplets, the average line broadening is equal to the perturbation prediction up to the limit of $\omega_{ex}/A_0\gamma$ studied. For three- and five-line spectra, integrated intensity moves from outer to inner lines while the total intensity remains equal to I_{total}.

5.2 Hyperfine Multiplet Coalescence and Narrowing

In a very old paper [14], we studied the narrowing of a 19-line proton hyperfine multiple indirectly by measuring the Gaussian content of the inhomogeneously broadened central line of di-*tert*butylnitroxide. We studied the central line, avoiding the complication of the dispersion components. The unresolved lines were modeled with a Gaussian–Lorentzian sum function which is an excellent approximation to a Voigt line shape function [2], showing that the experimental lines were well approximated by Voigt line shapes. We knew that the lines broadened and shifted differentially in the slow-exchange limit, but we reasoned that an average broadening would emerge from the Lorentzian component and an average proton hyperfine spacing from the Gaussian. Our mental picture of the narrowing mechanism was that the lines shifted toward each other until they collapsed leaving a narrow Lorentzian line. This is essentially what occurs in the case of ^{15}N where the line spacing rapidly approaches zero near $\omega_{ex}/\gamma A_0 = 1$.

However, it is now clear that our reasoning was faulty; the process is more complicated than that even for three lines. The decrease in the height of the outer

absorption lines contributes substantially to the narrowing of the spectrum and when those lines become negative, that contributes even further. Thus, in Fig. 10a, the collapsed line narrows (solid diamonds) by 44%, while the hyperfine spacing decreases by only 20%.

5.3 Transition to the Fast Spin-Exchange Limit

The present work details a method to obtain ω_{ex} well past the point at which the hyperfine multiplets coalesce into one line, but falls short of covering the entire range. For the fast spin-exchange limit, $\omega_{ex}/\gamma A_0 \gg 1$, the well-known expression for the narrowing of absorption spectra, first derived by Anderson and Weiss [15], was cast into a form appropriate for hyperfine multiplets by, for example, Eq. 3.27 of Ref [3]. Evaluating the constants, we have the following:

$$(\omega_{ex}/\gamma) = \frac{0.770}{\left[\Delta H_{pp}^{narrow}(\omega_{ex}) - \Delta H_{pp}(0)\right]}, \quad \text{for } ^{14}\text{N} \tag{20a}$$

$$(\omega_{ex}/\gamma) = \frac{0.289}{\left[\Delta H_{pp}^{narrow}(\omega_{ex}) - \Delta H_{pp}(0)\right]} \quad \text{for } ^{15}\text{N}, \tag{20b}$$

Referring back to Fig. 10, the solid diamonds are the measured values of $\left[\Delta H_{pp}^{narrow}(\omega_{ex}) - \Delta H_{pp}(0)\right]/A_0$. The computed values of $\omega_{ex}/\gamma A_0$ from Eq. (20) may be compared with the known input values to assess their accuracy. We find that at $(\omega_{ex}/A_0\gamma)_{upper}$, Eq. (20) is in error by 35% for ^{15}N and 8% for ^{14}N. For ^{15}N, the error is reduced to 8% at $\omega_{ex}/\gamma A_0 = 1.97$ and only reaches a reasonable 3.7% at $\omega_{ex}/\gamma A_0 = 5.90$. For ^{14}N, the error is reduced to 2% at $\omega_{ex}/\gamma A_0 = 4.10$. Assuming a broadening constant of $K_{ex}/\gamma = 150$ G/M for ^{14}N, typical for a low-viscosity liquid at elevated temperatures [8], the following concentrations are needed to achieve accuracies indicated in the parentheses: ^{15}N 0.085 M (35%); 0.170 M (8%); and 0.500 M (3.7%). For ^{14}N, one needs 0.160 M (8%) and 0.330 M (2%).

Let us take 8% is a tolerable error where we may say that the transition is complete. For ^{14}N, the transition is already complete at $(\omega_{ex}/A_0\gamma)_{upper}$, but, for ^{15}N, there is a gap between $(\omega_{ex}/A_0\gamma) \approx 1$–2.

5.4 Hypothesis

We offer the following hypothesis: Eq. (16) and the derivative of the real part of Eq. (1) are the same function. The two have the same domain, the real numbers, produce only one output value for each set of input parameters, and the output values are the same for each function to within ± 1 in the least-significant of sixteen digits. Therefore, although we cannot prove it, we have provided sufficient evidence to form a hypothesis and hopefully entice some good theorist to prove it. Our argument is only valid to $(\omega_{ex}/A_0\gamma)_{upper}$.

It has been 56 years since Daniel Kivelson first published [16] a theory to describe spin exchange between free radicals in liquids. As his reason to "develop the theory of exchange effects in liquids in somewhat more detail", Kivelson cited

the "ingenious explanation of the dependence of EPR line widths on viscosity" by Pake and Tuttle [17] in terms of spin exchange [16]".

He was able to predict the effects of spin exchange in the limits of slow- or fast-exchange, but could not describe the entire range. Equation (1), a rigorous theory covering the entire range was given by Currin [4]. Then, there was a period of activity in which some of the greatest minds in EPR contributed experimentally and theoretically as detailed in References [3, 7] and references therein. In the intervening 54 years, we have had Eq. (1) which has been verified in considerable detail experimentally [7–9] except for the additional shifts due to HSE during the act of spin exchange [6], but in a form that did not give us analytical expressions or provide a satisfying mental image of the behavior of the individual lines as they collapsed and disappeared into the merged spectrum. Equation (16) provides that image: all of the original lines retain their identity and are very simple admixtures of absorption and dispersion line shapes. We can only claim this up to values of $(\omega_{ex}/A_0\gamma)_{upper}$ detailed above and only for 2, 3, or 5 lines; however, if our hypothesis can be proved, it would be the final phase of the work of many. It is clear that each line loses its identity with a particular spin state. We view the lines as somewhat like modes of the coupled spin system.

Note added after this manuscript was in final form: The idea that spectral lines may be decomposed into individual absorption and dispersion that has been emerging through the years in our lab has found theoretical support in an important recent publication by Salikhov where the appearance of dispersion contributions is "an intrinsic feature of the coherence evolution of collective modes in the presence of the coherence transfer induced by a relaxation process" [18].

6 Conclusions

Equations (1) and (16) are the same within 16-digit precision up to $(\omega_{ex}/A_0\gamma)_{upper} = 0.99908$ for ^{15}N and to $(\omega_{ex}/A_0\gamma)_{upper} = 1.9882$ for ^{14}N, thus allowing interpretation of the spectra in terms of absorption–dispersion admixtures. The unweighted average broadening of the lines is identical to the perturbation prediction. Shifting of intensity from the outer lines to the central line for ^{14}N is reconfirmed such that all of the intensity resides in the central line at $\omega_{ex}/A_0\gamma = 2/\sqrt{3}$. At higher spin-exchange frequencies, the outer lines are of negative intensity while that of the central line is larger than the total intensity.

Acknowledgements The authors wish to thank Dr. K. M. Salikhov for numerous fruitful discussions and for suggesting the term "modes of the spin-coupled system". M.P. gratefully acknowledges support from NIH Grant SC3GM099635.

References

1. B.L. Bales, M. Meyer, S. Smith, M. Peric, J. Phys. Chem. A **113**, 4930–4940 (2009)

2. B.L. Bales, in *Biological Magnetic Resonance*, ed. by L.J. Berliner, J. Reuben (Plenum, New York, 1989), pp. 77–130
3. Y.N. Molin, K.M. Salikhov, K.I. Zamaraev, *Spin Exchange Principles and Applications in Chemistry and Biology* (Springer, New York, 1980)
4. J.D. Currin, Phys. Rev. **126**, 1995 (1962)
5. K.M. Salikhov, J. Magn. Reson. **63**, 271–279 (1985)
6. B.L. Bales, M. Meyer, S. Smith, M. Peric, J. Phys. Chem. A **112**, 2177–2181 (2008)
7. B.L. Bales, M. Peric, J. Phys. Chem. B **101**, 8707–8716 (1997)
8. B.L. Bales, M. Peric, J. Phys. Chem. A **106**, 4846–4854 (2002)
9. B.L. Bales, M. Peric, I. Dragutan, J. Phys. Chem. A **107**, 9086–9098 (2003)
10. H.J. Halpern, M. Peric, C. Yu, B.L. Bales, J. Magn. Reson. **103**, 13–22 (1993)
11. B.L. Bales, F.L. Harris, M. Peric, M. Peric, J. Phys. Chem. A **113**, 9295–9303 (2009)
12. B.L. Bales, K.M. Cadman, M. Peric, R.N. Schwartz, M. Peric, J. Phys. Chem. A **115**, 10903–10910 (2011)
13. B.L. Bales, M. Meyer, M. Peric, J. Phys. Chem. A **118**, 6154–6162 (2014)
14. B.L. Bales, D. Willett, J. Chem. Phys. **80**, 2997–3004 (1984)
15. P.W. Anderson, P.R. Weiss, Rev. Mod. Phys. **25**, 269–276 (1953)
16. D. Kivelson, J. Chem. Phys. **33**, 1094–1106 (1960)
17. G.E. Pake, T.R. Tuttle Jr., Phys. Rev. Lett. **3**, 423 (1959)
18. K.M. Salikhov, Appl. Magn. Reson. **47**(11), 1207–1227 (2016). **(Published online 24 September (2016))**